



Article

Estimation of Gully Growth Rate and Erosion Amount Using UAV and Worldview-3 Images in Yimeng Mountain Area, China

Guanghe Zhang ^{1,2}, Weijun Zhao ^{2,*}, Tingting Yan ³, Wei Qin ⁴ and Xiaojing Miao ⁵¹ School of Ecology and Environment, Southwest Forestry University, Kunming 650224, China² Key Laboratory of Tourism and Resources and Environment in Shandong Province, Taishan University, Tai'an 271000, China³ School of Civil and Architectural Engineering, Shandong University of Technology, Zibo 255000, China⁴ State Key Laboratory of Simulation and Regulation of Water Cycle in River Basin, China Institute of Water Resources and Hydropower Research, Beijing 100048, China⁵ Water Resources and Soil Conservation Service Center of Tai'an, Tai'an 271000, China; miaoxiaojing@ta.shandong.cn

* Correspondence: zwj_0920@tsu.edu.cn

Abstract: Non-homogeneous soil's high gravel content (also known as the "soil-rock dual structure") may render it more prone to erosion and the significant development of gullies. In order to reveal the morphological characteristics and erosion rate of gullies in "soil-rock dual structure" areas, this study focused on the Shagou Reservoir basin in the Yimeng mountain area as the study area. Based on a complete digital orthophoto map (DOM, 0.03 m) and a digital elevation model (DEM, 0.03 m) acquired by an unmanned aerial vehicle (UAV), the researchers calculated the length (L), top width (TW), depth (D), area (A) and volume (V) of 19 gullies and built and optimized the volume estimation model. The DOM and the DEM were used to modify the morphological parameters of 43 gullies extracted from high-resolution remote sensing (RS) stereopair images (Worldview, 0.5 m), and the development and evolution of gully erosion were evaluated in large scale. The results showed that: (1) after correction, the average relative errors of parameters L , TW, D and A computed from the UAV data and the high-resolution RS stereopair image data fell below 0.005%; (2) the mean of TW/ D was 5.20, i.e., the lateral erosion development of gullies far outweighed the downcutting erosion. The retrogressive erosion, lateral erosion and downcutting erosion rates of gullies were 0.01–0.83 m/a (averaged at 0.23 m/a), 0.01–0.68 m/a (averaged at 0.25 m/a) and 0.01–0.19 m/a (averaged at 0.09 m/a), respectively, between 2014 and 2021; (3) the volume-area (V - A) model for gullies is the optimal one ($p < 0.01$, $R^2 = 0.944$). A total of 90.7% of the gully volume was growing at an erosion rate of 0.42–399.39 m³/a and the total erosion rate of the gullies was 3181.56 m³/a from 2014 to 2021. These research findings can serve as a basis for the quantitative modeling of gully erosion in water-eroded locations with a large-dimension "soil-rock dual structure".

Keywords: gully; erosion rate; multisource remote sensing; soil-rock dual structure; Yimeng mountain area

Citation: Zhang, G.; Zhao, W.; Yan, T.; Qin, W.; Miao, X. Estimation of Gully Growth Rate and Erosion Amount Using UAV and Worldview-3 Images in Yimeng Mountain Area, China. *Remote Sens.* **2023**, *15*, 233. <https://doi.org/10.3390/rs15010233>

Academic Editor: Emilio Rodriguez Caballero

Received: 25 October 2022

Revised: 28 December 2022

Accepted: 28 December 2022

Published: 31 December 2022



Copyright: © 2022 by the authors. Licensee MDPI, Basel, Switzerland. This article is an open access article distributed under the terms and conditions of the Creative Commons Attribution (CC BY) license (<https://creativecommons.org/licenses/by/4.0/>).

1. Introduction

Water and soil loss due to soil erosion has severely restricted the development of local economies [1–3]. Gullying is the major soil erosion in many areas of the world [4,5]. World-wide gullying has caused a degeneration of productive land over approximately ten million square kilometers and an annual economic loss of up to USD 231 billion [3,6,7]. Gully erosion is a form of gullying, whose evolution process and erosion rate hinge markedly on soil texture and lithology [8–10]. On the one hand, nonhomogeneous soil with a high content of gravel may facilitate the infiltration of water and reduce the acting force of overland runoff on the gully [4]; on the other hand, it may lead to stony desertification and an increase in its sensitivity to erosion [11]. Therefore, a shallow soil layer, high content of gravels in the soil and the extensive development of gullies are the unique characteristics

of the “soil-rock dual structure”. However, the evolution of gully morphology and the dynamic change in the erosion volume of gullies remain unclear. Meanwhile, the development of gullies is rarely studied in the “soil-rock dual structure” area, which has seriously restricted the sustainable development of regional agriculture and the construction of the ecological environment.

Over the recent years, gully erosion has been monitored mostly by remote sensing (RS) technologies (e.g., high-resolution RS imagery, aerial photography, Light Detection and Ranging (LiDAR), 3D laser scanning, 3D photo reconstruction and oblique photogrammetry), field surveying and combined methods both at home and abroad [12–20]. Among them, high-resolution RS imagery is superior to other traditional surveying methods in accuracy and effectiveness, delivering relatively accessible and reliable data [21]. The continuously developing UAV technology has demonstrated such advantages as low cost, high precision, high sensitivity, wide range and high efficiency and promised enormous potential in landscape mapping and geomorphic surveying [22,23]. While topographic data are acquired, the point cloud of the structure from the motion (SfM) of the UAV is nicely matched with the point cloud of LiDAR, at high precision [22]. In recent years, UAV photogrammetric technology has been widely applied in spatial modeling and the erosion monitoring of gully systems in many countries and regions [4,24–26]. The combination of UAV oblique photogrammetric technology and high-resolution RS imagery is of special value in the monitoring of the variations in gully length, width, area and volume [4]. Zhang et al. [27] used Google images and UAV images from the Loess Plateau region to accurately predict the severity and leading factors of road erosion. Gullies have developed extensively in the Yimeng mountain area with a “soil-rock dual structure” due to the impacts of slope cropland and other human activities. However, few reports have ever covered the gully erosion monitoring in this area. It is not clear whether it is feasible to apply UAV photogrammetric data to modify the morphological parameters of gullies extracted from high-resolution remote sensing stereo images to monitor the development of gully erosion in a larger scale.

The calculation of gully erosion rate is implemented mainly by RS images with comparable resolutions and accuracies over different periods. Typically, the average erosion rate within a period is obtained by calculating the differences in gully length, width, depth, area, volume and other parameters [16,28]. The gully length and area are accessible from RS images, but the measurement of erosion volume is controversial to some extent, and the estimation of volume needs further development [4,13]. Therefore, the relation between volume and each morphological parameter has become a research hotspot. Existing studies show that the volume of gully erosion can be calculated by building a volume estimation model based on morphological parameters [12,19,29–33]. However, due to the differences in topography, precipitation, lithology, soil property, land-use type and other environmental characteristics and in gully development scale, the fitting relationship and coefficient between gully volume and each parameter are largely different across China [32,34,35], Ethiopia [12,19,36], Spain [30], Nigeria [33], Iran [37] and other study areas. The relationships between gully volume and gully length, area and other morphological parameters remain unclear in regions where the soil texture has a typical “soil-rock dual structure”, restricting the evaluation research of its erosion rate and the dynamic change in erosion volume.

Therefore, this study aims to explore the development and evolution and volume estimation model of gullies with a typical “soil-rock dual structure” in the Yimeng mountain area for quantitative erosion simulation. The probe into the relationship between the morphological parameters and the development rate of gullies provides a new idea for the research of gully erosion in water-eroded areas with a “soil-rock dual structure”. This study takes the gullies of the Shagou Reservoir basin in the Yimeng mountain area of China as the research object. In this study, a complete digital orthophoto map (DOM, 0.03 m × 0.03 m) and a digital elevation model (DEM, 0.03 m × 0.03) of the gullies were built by UAV-enabled oblique photography to calculate the morphological parameters, and

a gully volume estimation model was established through screening. The morphological parameters of the gullies extracted from the high-resolution RS images in two periods of 2014 and 2021 were corrected through applying the morphological parameters and data acquired by the UAV. The results of the study provide a theoretical basis not only for research on gully erosion development and evolution in the Yimeng mountain area but also for the quantitative modeling of gully erosion in water-eroded regions with a “soil-rock dual structure”.

2. Materials and Methods

2.1. Study Area Overview

Located in the south-central part ($36^{\circ}06'04''\text{N}$ – $36^{\circ}08'57''\text{N}$, $118^{\circ}38'01''\text{E}$ – $118^{\circ}39'59''\text{E}$) of the Yimeng mountain area, the Shagou Reservoir basin in Yishui County (Figures 1 and 2a,b), Shandong Province is a typical northern hilly and mountainous area, where the soil texture features the typical “soil-rock dual structure” [38]. In the study area, the bedrock is predominated by limestone, and the soil types include skeletal soil (majority), with more gravel, loose soil and shallow soil layers. Through investigation, the soil rock ratio of the gullies was found to be evenly distributed within the range of 0–5 in the study area. The 2–5 mm gravel content is the highest (24.94%) of the total gravel content (37.33%) (Figure 2e) [39]. The entire study area covers 6.8 km^2 , at an altitude of 310–340 m; it has a continental monsoon climate in the warm temperature zone, with an annual average temperature of about $13\text{ }^{\circ}\text{C}$, annual average precipitation of 700–900 mm; precipitation is concentrated, mostly in the summer flood season (June–September) and dominated by rainstorms, with great interannual variation. The main arbor species include *Populus tomentosa* and *Robinia pseudoacacia*. The study area is dominated by slope croplands and woodlands, followed by garden plots and other land types.

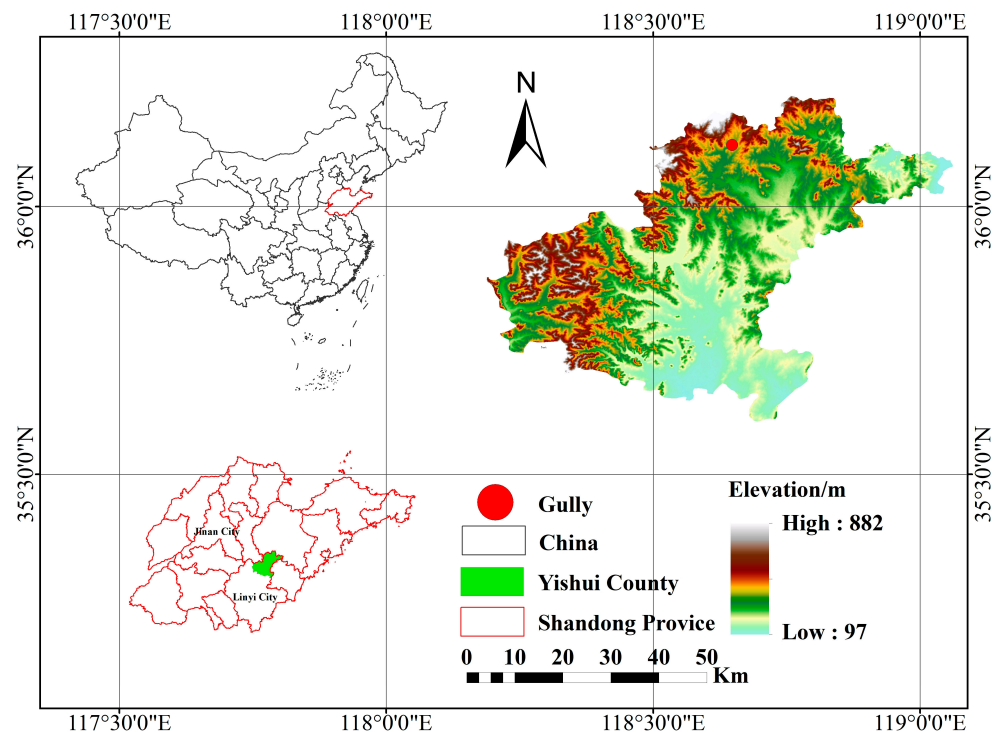


Figure 1. Location of the study area.

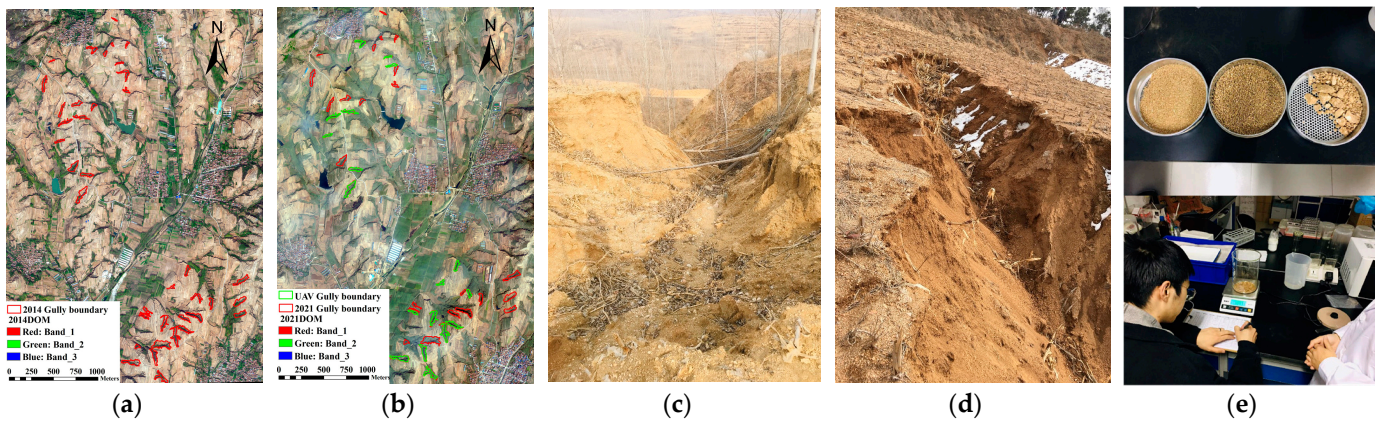


Figure 2. Gully distribution and introduction. (a,b) Map of gully distribution in high-resolution remote sensing stereo image pairs (ground sampling distance: 0.50 m) in 2014 and 2021, respectively. (c,d) Sample of a typical gully. (e) Experiment on soil-rock dual structure.

2.2. Multisource RS Data Acquisition and Processing

The research methods mainly adopted in this study were (Figure 3): (i) gully morphology parameters were obtained through UAV data, and the optimal volume model was constructed and verified; (ii) gully morphology parameters in the study area were obtained through high-resolution remote sensing images combined with the volume model; (iii) the analysis of gully morphology parameters was undertaken by UAV and high-resolution remote sensing images and a correction model; (iv) the corrected gully morphology parameters were obtained and the development rate was calculated through two high-resolution remote sensing images. The specific data processing methods were as follows.

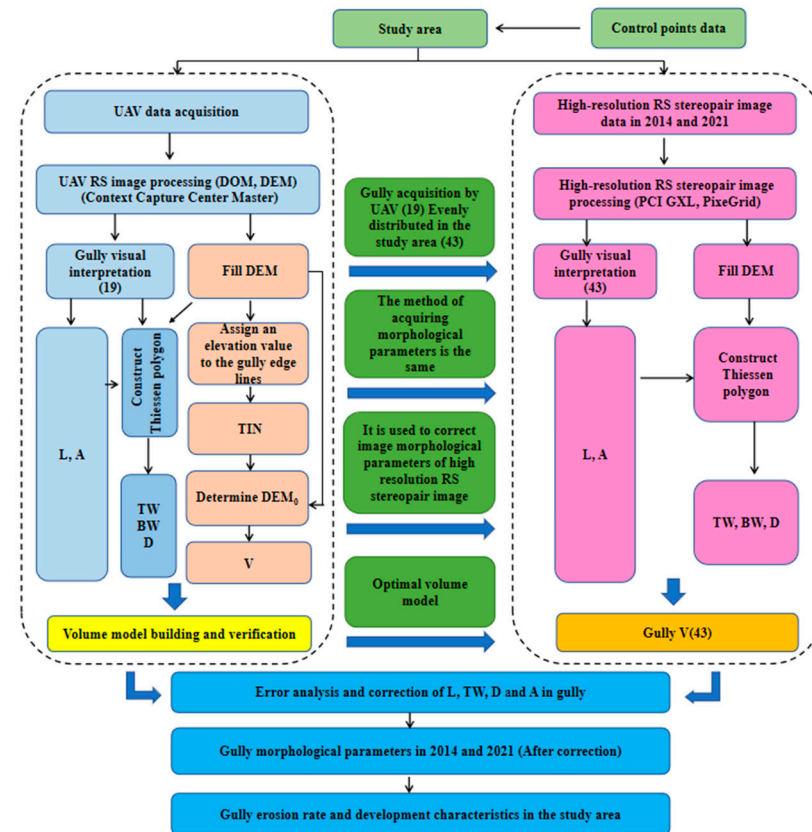


Figure 3. Flowchart of research.

2.2.1. UAV Data Acquisition and Processing

The image data acquired by the UAV have a high resolution (0.03 m). However, the UAV equipped with an oblique photographing camera consumes power rapidly in flight, and it can scan only a small area per flight. It would take a long time to obtain a sufficient number of gully image data by flying such a UAV. To reduce the effects of the vegetation and snow over the gullies in the Yimeng mountain area on the accuracy of the DEM data, mid-March 2021 was selected as the study period, when the vegetational noise was lowest and there was no snow on the ground. All UAV flights were carried out between 8:30 and 15:30 at a low wind speed and in a clear sky. An oblique photographing camera (model: FAST X1, single lens pixel: 24.3 million, focal length of lens: 35 mm \times 5, mapping scale $>$ 1:500, comes with RTK, external pos) was mounted on a Dajiang Matrice 600 Pro UAV (SZ DJI Technology Co., Ltd., Shenzhen, Guangdong Province, China). The UAV hovered at a height of 150 m and the ground resolution was set to 2.5–3.0 cm. The front and side overlaps were, respectively, 80% and 75%.

The RTK-GPS had been used to detect 15 control points within the study area for UAV-enabled RS image correction before the UAV was located with an oblique photographing camera to take five groups of photos (8606 \times 5) at a height of 150 m. Based on the software Context Capture Center Master, the control points and pos data were imported to generate the photos taken by the UAV into orthoimages, a digital elevation model (DEM) and a 3D model. Through photomosaic processing, a complete digital orthophoto map (DOM, 0.03 m \times 0.03 m) and the DEM (0.03 m \times 0.03 m) were created, from which gully edge lines could be extracted for the calculation of the gully area.

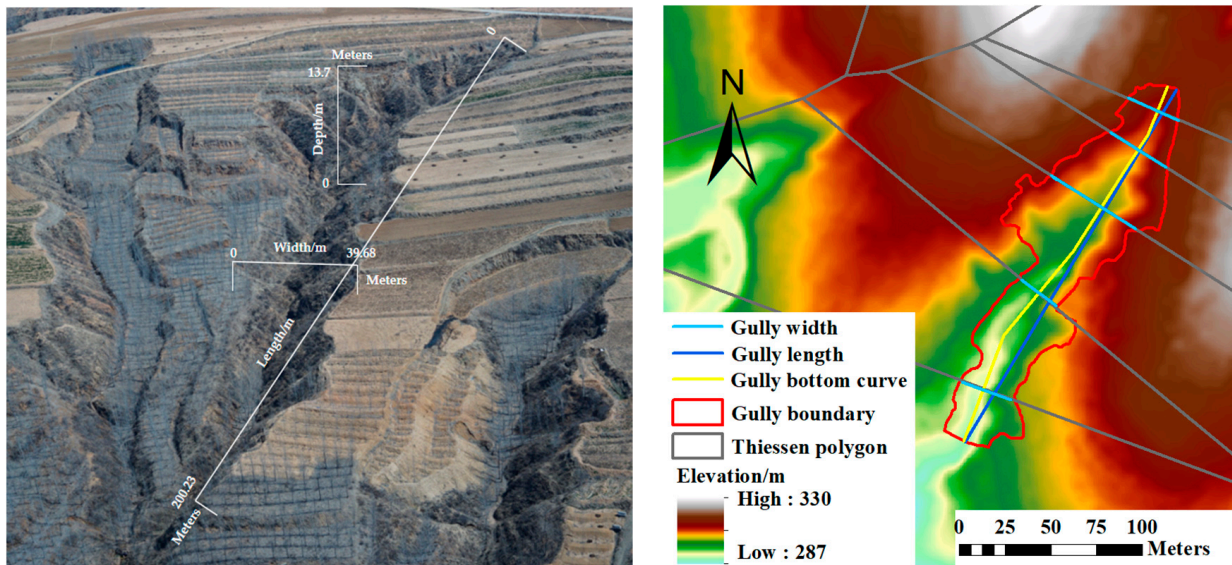
2.2.2. High-Resolution RS Stereopair Image Processing

The high-resolution RS images (Worldview-3 (OR2A, 0.5 m)) with stereopairs in the two periods March 2014 and February 2021 were used, including satellite panchromatic data, a base map, elevation data and multi-band satellite data. The pre-processing procedure mainly includes the following steps. First, in the PCI geographic imaging accelerator (PCI GXL) software, the detected control points are used for geometric correction. Next, the pan-sharpening method is used for image fusion pre-processing, and then ortho-graphic correction. Finally, Photoshop software is used to homogenize, inlay and crop the images and finally generate a complete DOM (0.5 m \times 0.5 m). In the process of DEM production, the first step is space-three encryption with PixeGrid software. Then, stereo image pairs are created based on image orientation and kernel line generation, and a regional digital elevation model is built through algorithm matching. Finally, the complete DEM is generated through human-computer interaction editing, inlaying and cropping.

2.3. Acquisition and Verification of Morphological Parameters of Gullies and Volume Calculation

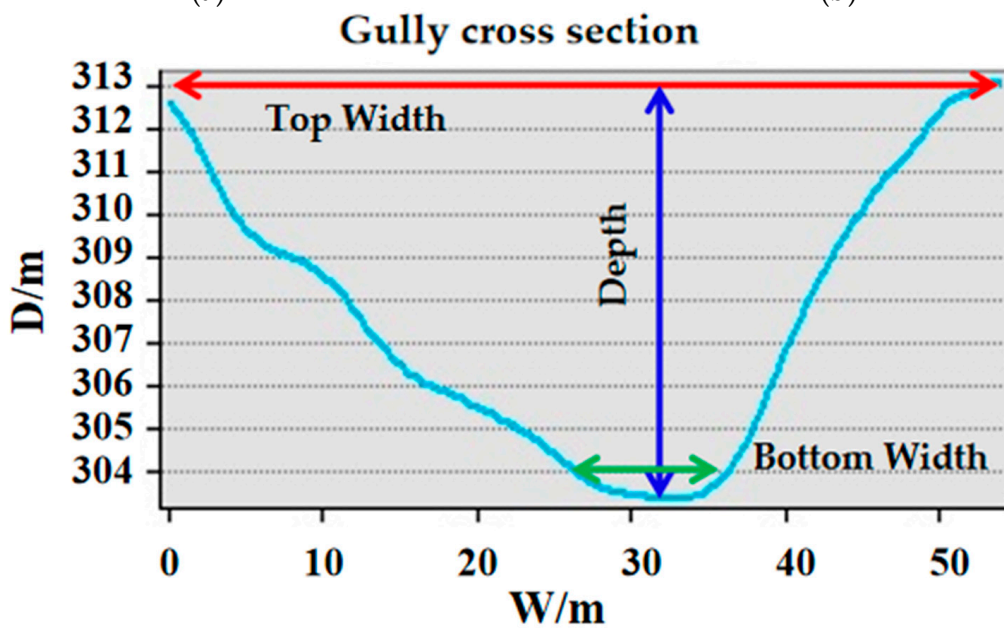
A gully develops through erosion on a single slope. Its longitudinal profile is not parallel to the slope, and its main body is below the gully edge line [40]. Based on the oblique photography data from the UAV, the morphological parameters length (L), top width (TW), bottom width (BW) (The ratio TW/BW gives the type of each gully), depth (D) and area (A) of 19 gullies were extracted to verify the precision of the high-resolution RS imagery and build the corrective model. The gully L , TW , D and A obtained from the UAV RS image and high-resolution RS image were used to construct the correction model, and the error correction of morphological parameters obtained from the high-resolution remote sensing image was carried out to make it more accurate. Therefore, 19 uniformly distributed gullies were randomly selected for flight data collection, and then the morphological parameters of these gullies collected by the UAV were used to correct the morphological parameters extracted from the high-resolution RS stereopair images in the study area (Figure 2b). The straight-line distance from the gully head to the mouth was taken as the gully length. A curve was made along the contour line of the gully bottom, and a Thiessen polygon was constructed to obtain 4–9 cross sections, and accordingly the parameters TW , BW and D . Their mean was calculated (Figure 4) [41].

Meanwhile, the gully volumes were calculated by the following procedure. Through the depression-filling treatment of the complete DEM generated from UAV data, an elevation value is first assigned to the gully edge lines to generate a triangular irregular network (TIN). Next, a DEM is constructed and clipped. Finally, the original erosion surface of the gullies (DEM_0) is determined [42–44]. The above parameters could be acquired based on the DEM and the DEM_0 of the gullies.



(a)

(b)



(c)

Figure 4. (a–c) Example of typical gully length, width, depth and cross section.

The gully volume (V) was estimated in terms of the higher-precision parameters L , TW , BW , D and A . The gullies in the study area were investigated on the spot through the close observation of their characteristics. The gullies with a typical morphology (wedge shape, lane shape or palm shape) and an obvious gully edge line were visually interpreted, and their distribution was reflected in the high-resolution RS images [45]. Through the same procedure, the morphological parameters L , TW , BW , D and A of 43 gullies were extracted from the DEM and DOM data acquired from the two periods of high-resolution

RS stereopair images for building a gully volume estimation model in large dimensions and calculating the gully erosion rate. The length, width and area of the gullies in the study area range within 35–250 m, 5–55 m and 500–1300 m², respectively, with the medians being 120 m, 23 m and 3189 m², respectively (Figure 2c,d).

2.4. Model Verification Method

The accuracy of the volume estimation model was evaluated in terms of average relative error (E_r) and Nash-Sutcliffe efficiency (E_{ns}) [46], which are calculated, respectively, by the following formulae:

$$E_r = \frac{1}{n} \sum_{j=1}^n \left| \frac{M_j - P_j}{M_j} \right|, \quad (1)$$

$$E_{ns} = 1 - \frac{\sum_{j=1}^n (M_j - P_j)^2}{\sum_{j=1}^n (M_j - M_m)^2}, \quad (2)$$

where M_j is the measured volume of the j th gully; P_j is the predicted volume of the j th gully; M_m is the mean of the measured volumes. The smaller the value of E_r or the greater the value of E_{ns} , the closer the model's predicted value to the measured value.

3. Results

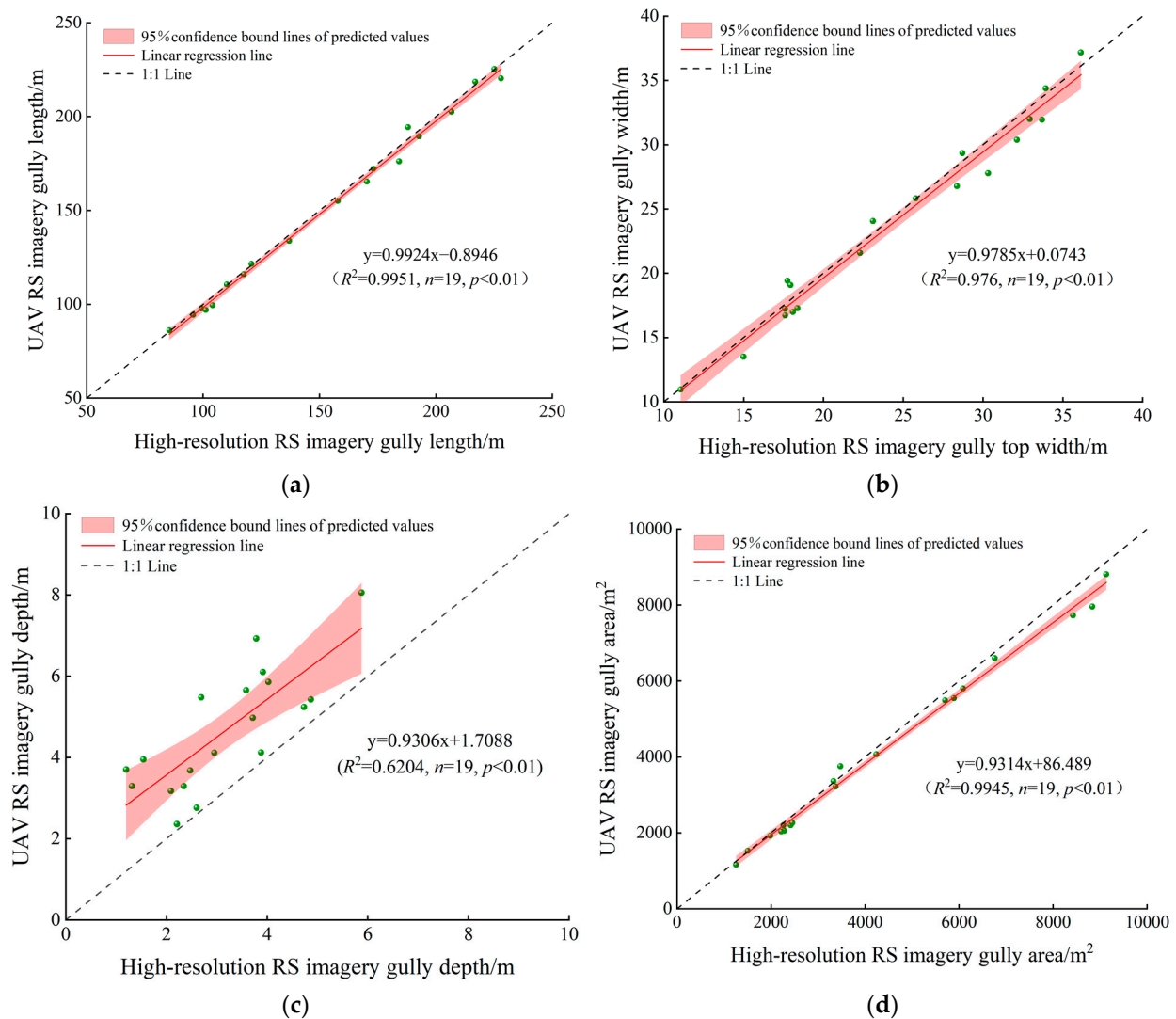
3.1. Precision Analysis and Correction of Morphological Parameters of Gullies Extracted from High-Resolution RS Stereoscopic Images

To verify the precision of the high-resolution RS imagery interpretation of the gullies, a comparative analysis was conducted on and between the errors of the morphological parameters of the gullies interpreted by the UAV imagery and by the high-resolution RS imagery. The overall error ranges between 0.09% and 32.12%. The more significant errors occur in the maximum, overall value and mean of D , all of which exceed 26%, while the errors of all other morphological parameters are below 10%, mostly concentrated below 5%. The average errors of 19 gully L , TW , D and A are 2.06 m, 0.45 m, 1.49 m and 208.09 m², respectively. Moreover, the maximum errors of single gully L , TW , D and A are 8.18 m, 2.54 m, 3.14 m and 877.50 m², respectively; the minimum errors are 0.21 m, 0.03 m, 0.15 m and 14.96 m², respectively. The relative errors of total L , TW , D and A are 1.36%, 1.88%, 32.12% and 5.09%, respectively, and are 39.08 m, 8.49 m, 28.32 m and 3953.67 m². The values of L , TW and A acquired by high-resolution RS imagery are larger than their actual values, while the value of D is smaller than its actual value (Table 1). The main reason is the vegetation coverage at the bottom of some of the gullies, leading to a small depth of interpretation based on the high-resolution RS stereopair images and to a large error.

To acquire higher-precision morphological parameters for the evaluation of the development and evolution of the gullies, a linear regression model was built for L , TW , D and A acquired separately by visual interpretation high-resolution RS imagery and by UAV RS imagery (Figure 5) for error correction. The average relative errors all fell below 0.005% after correction. After correction, the accuracy of the average L , TW , D and A of the 19 gullies was improved by 2.05 m, 0.45 m, 1.49 m and 207.88 m², respectively. Eventually, higher-precision morphological parameters L , TW , D and A of gullies based on high-resolution RS imagery were acquirable separately using the corrective model. The accuracy of the total L , TW , D and A of the gullies in 2014 and 2021 was improved by 164.92 m, 37.37 m, 128.28 m and 14,947.91 m², respectively. Moreover, the accuracy of single gully L , TW , D and A was improved by 1.20–2.64 m, 0.09–1.11 m, 1.19–1.67 m and 0.74–812 m², respectively.

Table 1. Statistics on the morphological characteristics of gullies interpreted by UAV imagery and high-resolution RS imagery ($n = 19$).

Image	UAV Image	RS Image	Error	Image	UAV Image	RS Image	Error
Length max/m	225.32	225.11	0.09%	Depth max/m	8.05	5.88	26.96%
Length min/m	86.08	85.48	0.70%	Depth min/m	2.36	2.21	6.42%
Total length/m	2875.46	2914.54	1.36%	Total depth/m	88.15	59.83	32.12%
Average length/m	151.34	153.40	1.36%	Average depth/m	4.64	3.15	32.12%
Width max/m	37.16	36.14	2.74%	Area max/m ²	8808.67	9131.90	3.67%
Width min/m	10.96	11.06	0.91%	Area min/m ²	1160.70	1257.08	8.30%
Total width/m	452.37	460.86	1.88%	Total area/m ²	77,691.33	81,645.00	5.09%
Average width/m	23.81	24.26	1.88%	Average area/m ²	4089.02	4297.11	5.09%

**Figure 5.** Linear regression model for error correction of 3D morphological parameters of the gullies: (a) Gully length error correction; (b) Gully top width error correction; (c) Gully depth error correction; (d) Gully area error correction.

3.2. Development Rate of Gullies in Yimeng Mountain Area

3.2.1. Development Rate of Retrogressive Erosion of Gullies

As calculated based on the high-precision gully length data after correction, the total gully lengths in 2014 and 2021 are 5693.49 m and 5718.64 m, corresponding to the average lengths of 132.41 m and 132.99 m, respectively. Amid the 7a, 65.12% of the 43 gullies experienced an increase in length. Considering the gullies alone that experienced the increase in length (Figure 6), 57.14% had a length increment of greater than 1 m, and the development rate of gully length ranges within 0.01~0.83 m/a, and that of an average gully's length was 0.23 m/a (Table 2).

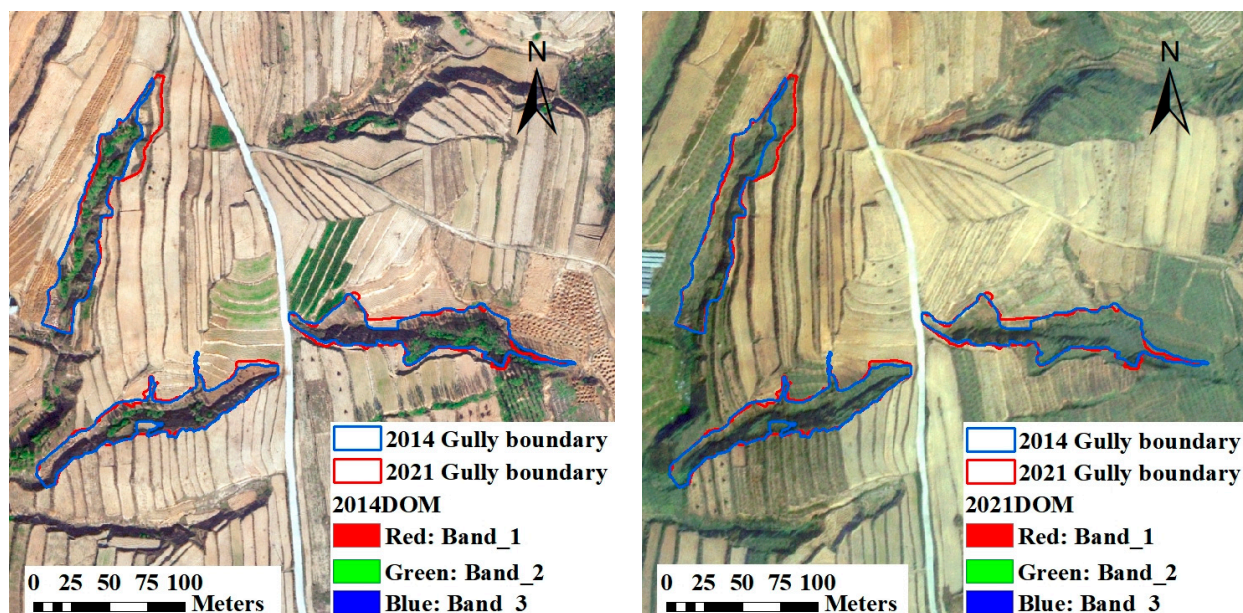


Figure 6. An example of gully length increase.

Table 2. Annual variation in gully length during 2014–2021 ($n = 28$).

Statistic	2014 Gully Length/m	2021 Gully Length/m	Gully Linear Growth Rate/($m \cdot a^{-1}$)	Linear Growth Ratio/%
Maximum	221.22	222.50	0.83	6.73
Minimum	39.23	39.58	0.01	0.03
Mean	120.27	121.89	0.23	1.53
Median	104.40	105.01	0.17	1.16
Total	3367.52	3413.04	6.50	1.35

The gullies under investigation total 43, 28 of which have experienced an increase in length.

3.2.2. Development Rate of Lateral Erosion of Gullies

This study established a Thiessen polygon for the vector boundaries and curve lengths of the bases of the 43 gullies, selected 534 cross sections to calculate the TW and D of the gullies on the high-resolution RS images of the two periods, and then obtained the corrected values of TW and D . Amid the 7a, the 43 gullies experienced an increase of 54.13 m in total TW, or equivalently an average gully experienced an increase of 1.26 m in width; 81.39% of the gullies experienced an increase in width (Figure 7), with a maximum increase in width of 4.74 m, maximum decrease in width of 3.73 m and a median of 1.30 m. Considering the gullies alone that experienced the increase in width, the development rates of gully width range within 0.01~0.68 m/a, and that of an average gully's width is 0.25 m/a.

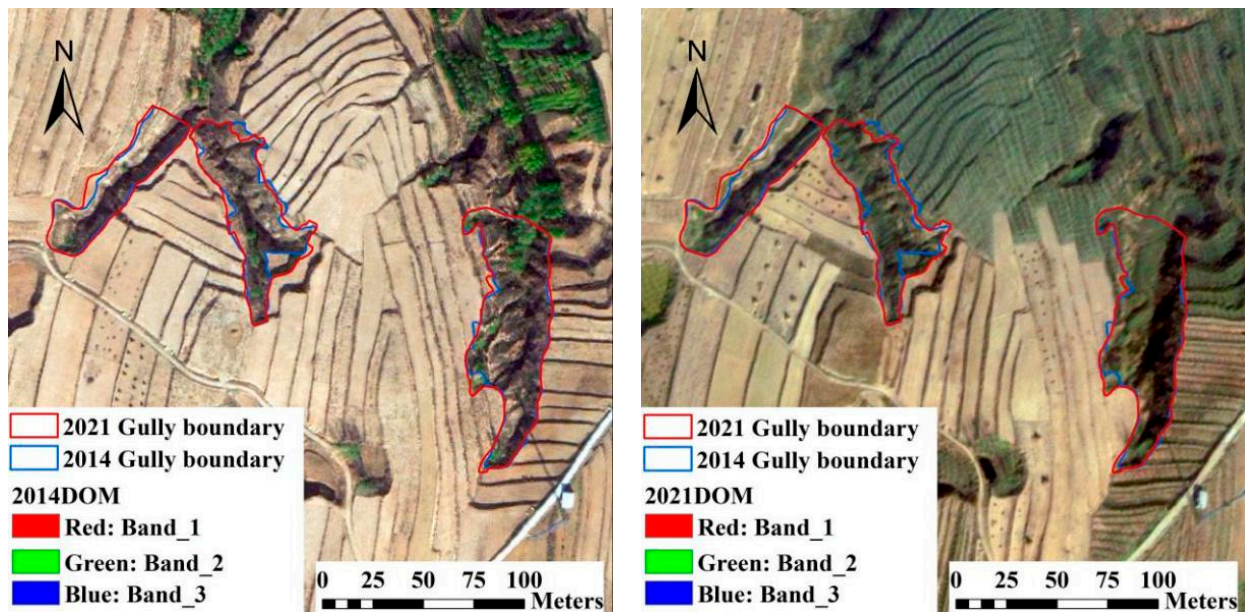


Figure 7. An example of gully width increase.

3.2.3. Development Rate of Gully Downcut

Amid the 7a, the 43 gullies experienced an increase of 0.04 m in total depth, and 53.5% of them experienced an increase in depth. A total of 79.1% of the gullies experienced variations in depth centralized between -1 m and 1 m, with a maximum increase in depth of 1.36 m, maximum decrease in depth of 2.46 m and a median of 0.14 m. Considering the gullies alone that experienced an increase in depth, the development rates of their depth range within 0.01~0.19 m/a, and that of an average gully's depth is 0.09 m/a.

The TW- D relation of the 43 gullies in 2021 was further figured out. The TW/ D values of the gullies range within 0.91~17.99, with a mean of 5.20 and greater than 1, with all points located to the upper left of the 1:1 line (Figure 8), showing that the lateral erosion rate is greater than the downcutting erosion rate of the gullies [47].

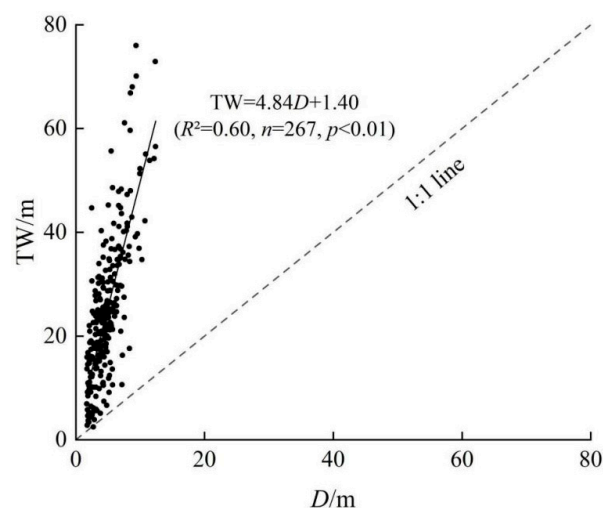


Figure 8. The TW- D relation of the gullies.

3.3. Optimal Gully Volume Model Building and Verification

Deng et al. classified the cross-sectional shape of gullies into shape V (0~0.4), shape V~U (0.4~0.6) and shape U (0.6~1.0) by the BW/TW value [47]. The gullies selected in this study have a BW/TW value ranging between 0.04 and 0.17, with a mean of 0.08, so all are

V-shape gullies. The erosion gully measurement technology has successfully recognized gullies with large width and depth, but the practice of volume estimation needs further development [13]. The volumes of the 19 gullies acquired by UAV RS imagery range from 1588.11 to 33,291.44 m³, averaged at 10,398.07 m³. A regression analysis was conducted on the L , TW , D and A of the 19 gullies acquired by UAV RS imagery versus the volume V of each gully (Figure 9). All the four morphological parameters are significantly related with V by some power function. Among them, the A - V regression relation is fitted by the formula $V = 0.0513 A^{1.4535}$, and it is the most significant ($R^2 = 0.944$). Through the above regression model, the gully volume was predicted, and the relative error (E_r) and Nash–Sutcliffe efficiency (E_{ns}) between the predicted and measured volumes were calculated (Table 3). The smaller value of E_r , greater value of E_{ns} and the coefficient of determination R^2 indicate the V - A model has a higher precision in predicting gully volume than the V - L and V - TW models, showing that gully area is a key factor of gully volume estimation in the Yimeng mountain area.

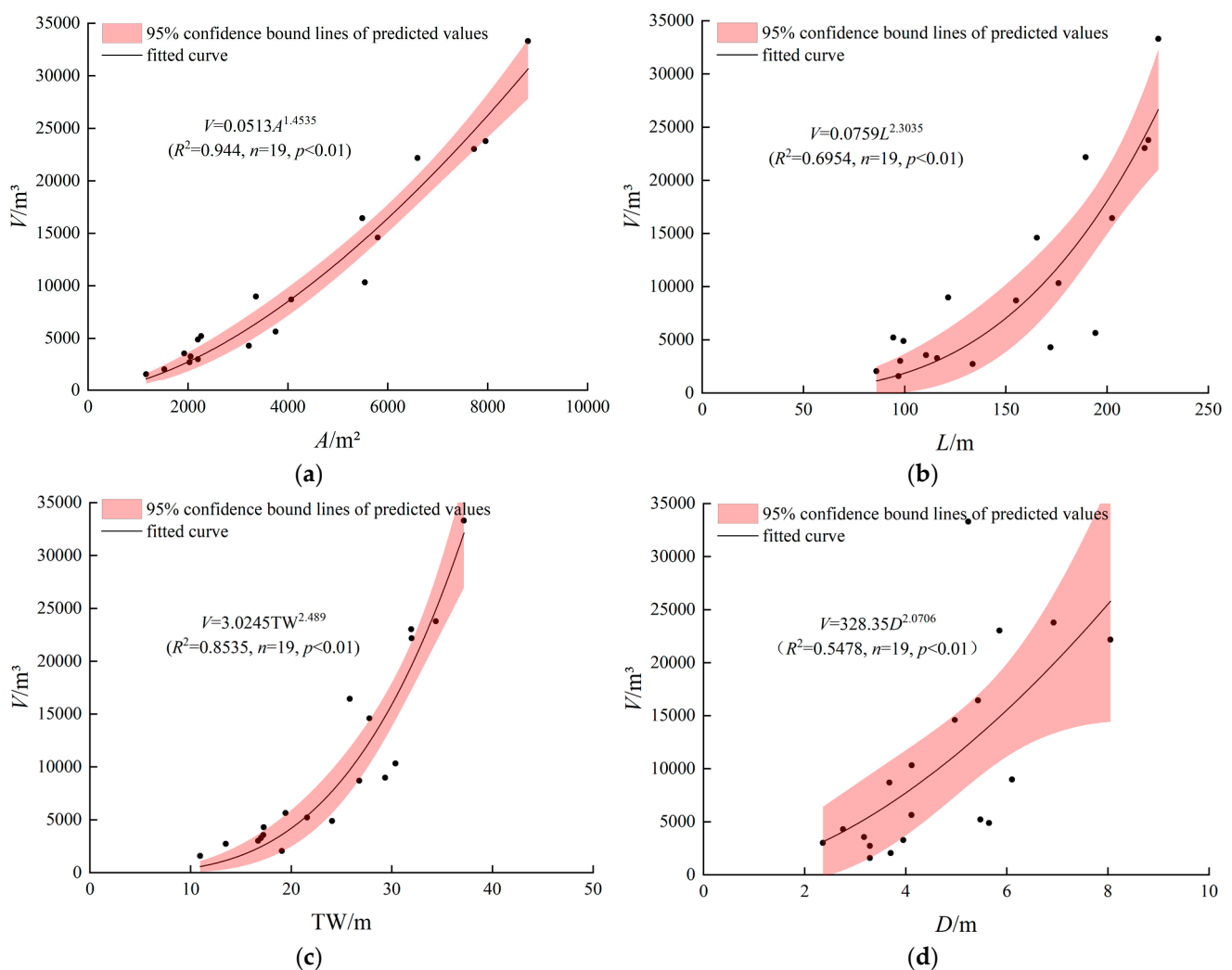


Figure 9. Relation between gully volume (V) and the main parameters by UAV RS imagery interpretation: (a) Gully volume—area relation; (b) Gully volume—length relation; (c) Gully volume—top width relation; (d) Gully volume—depth relation.

Table 3. Relative error (E_r) and Nash–Sutcliffe efficiency (E_{ns}) between measured gully volume and predicted gully volume.

Predicted Model	Total Measured Volume/m ³	Total Predicted Volume/m ³	E_r	E_{ns}	R^2
V-A	197,563.27	191,077.97	0.178	0.929	0.944
V-L		173,440.16	0.438	0.696	0.695
V-TW		179,900.83	0.293	0.786	0.854

3.4. Analysis of the Dynamic Change in Gully Erosion Volume

According to the V-A model, using the corrected gully area, it was estimated that 90.7% of the gullies in the study area experienced an increase in volume during 2014~2021, which is consistent with the variation in gully area (Table 4 and Figure 10). The annual increment in erosion volume of 39 of the gullies with increases in both area and volume ranges from 0.42 m³ to 399.39 m³, averaged at 81.58 m³. The gullies were graded and classified by annual erosion volume. A total of 10.26% of the gullies selected within this study area can be identified as middle-sized developing ones (annual erosion volume > 200 m³) [48], and the total erosion rate of all gullies within the study area is 3181.56 m³/a.

Table 4. Increments in area and volume of 39 gullies during 2014–2021.

Statistic	A/m ²		V/m ³		A Growth/m ²	A Growth Rate/(m ² ·a ⁻¹)	V Growth/m ³	V Growth Rate/(m ³ ·a ⁻¹)
	2014	2021	2014	2021				
Maximm	12,056.12	12,291.58	43,868.45	45,119.30	733.39	104.77	2795.71	399.39
Minimm	518.11	588.18	452.41	544.00	1.28	0.18	2.96	0.42
Means	3,535.42	3,710.00	8,598.70	9,169.75	174.59	24.94	571.05	81.58
Medians	2,830.65	3,188.92	5,338.68	6,348.38	140.07	20.01	415.01	59.29
Total	137,881.30	144,690.25	335,349.48	357,620.37	6808.95	972.71	22,270.89	3181.56

The gullies under investigation total 43, 39 of which experienced an increase in area and volume.

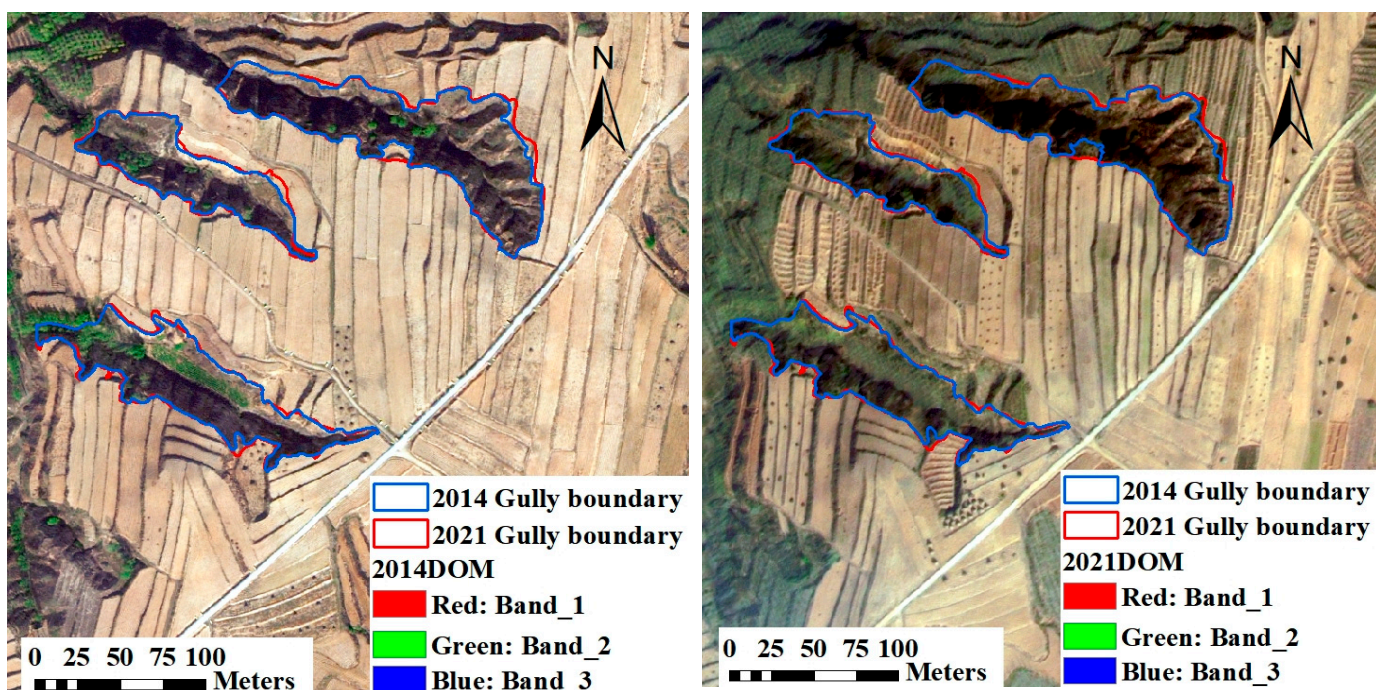


Figure 10. An example of gully area increase.

4. Discussion

The implementation of the dynamic monitoring of soil erosion is of vital significance in the Yimeng mountain area in North China, where the soil texture features a typical “soil-rock dual structure”. The research results show that V is more strongly correlated to A than to L , TW and D . This research finding is similar to those of Belayneh et al. [12] and Zhang Yan et al. [25] in Northwest Ethiopia and in the China Loess Plateau, respectively, despite a certain discrepancy. The values of A and V of the gullies within the study area are both greater than their counterparts in the northwestern part of the Ethiopian Highland and smaller than those in the loess hilly region. Such a discrepancy stems mainly from the fact that the historical trend of the gully extension researched by Belayneh et al. [12] is limited, hence the younger ages of the gullies, and that human measurements were taken during the development process to restrain the gully development scale in their study area. The gullies studied by Zhang Yan et al. [35] were developing in a larger scale in the loess area with loose soil texture. This study is oriented at the gullies developing in the “soil-rock dual structure” region, part of which features high gravel concentration or bare bedrocks, limiting the gully development rate, and the proportion of soil-rock structure could also have a certain inhibitive effect on gully development by accelerating water infiltration [4]. The V - A model derived in this study is shown in Figure 9a, where $a = 0.01513$, $b = 1.4535$ and the coefficient of determination $R^2 = 0.944$. The value of b is 1.04 to 1.28 times that in the northwestern part of the Ethiopian Highland and in other regions of China [12,28,31,32], suggesting a higher vulnerability and a greater rate of increase in gully depth per unit area of the gullies within the study area than in other homogeneous soil regions, with great variations in depth from the gully head to gully center to gully mouth [32,35].

The variability of the ratio BW/TW reflects the leading factors affecting the gully bottom width and gully shore spreading rate [19]. Referring to the research results of Deng et al. [44], this study selected the gullies with the ratio BW/TW ranging within 0.04~0.17, classified as V-shape gullies (0~0.4). Yibeltal et al. [19] studied the ratios BW/TW (0.18~0.85, 0.64~0.90 and 0.17~0.39) of three distinct agroecological environment gullies in Ethiopia. Under the effect of soil physical properties, the ranges of variations are all wider than those of the gullies in this study area, and the gully forms are complex. Unfortunately, the gully type in this study is simple, and the soil-rock content proportion in the soil remains vague, so the effect of the “soil-rock dual structure” on gully shore spreading calls for further exploration. The ratio TW/D reflects the gully section morphology [36], as well as the TW - D relation of gullies. The ratio TW/D of the gullies in this study area varied between 1.77 and 7.55 (mean 5.06), with the gully crosswise development rate overtaking the bottom downcutting erosion rate [47] in 2021. A similar TW/D value was found in the black soil region of Northeast China studied by Li et al. [32], while that found in the Ethiopian Highland from the research by Frankl et al. [36] and Yibeltal et al. [19] was smaller than the TW/D value in this study area. This discrepancy stems mainly from the differences in soil texture and land-use type. This study focused on the gullies developing on croplands, which were prone to crosswise erosion without corresponding preventive measures taken against the low vegetation coverage on their two sides. The soils at the gully head and on both sides of the gully slope have been washed into the gully bottom and deposited due to erosions such as runoff erosion and gravity collapse, resulting in the gully bottom deepening or shallowing. Indeed, the depth of most gullies varies from -1 m to 1 m.

During 2014~2021, the average development rates of the gullies in L , TW , D and V were 0.23 m/a, 0.25 m/a, 0.09 m/a and 81.58 m³/a, respectively, the retrogressive erosion rate was smaller than that of the eroded gullies in other homogeneous soil regions, the erosion volume was greater than that in other regions, and the development rate of lateral erosion was far greater than that of the dissected valleys in the loess hilly and gully region (Table 5). This suggests that the lateral erosion on both sides of gully slope dominated the retrogressive erosion and the downcutting erosion throughout the gully erosion development process in the Yimeng mountain area (Figure 11). Different from

the research results of Samani et al. [49] and Yibeltal et al. [19] in three agroecosystems in Southwest Iran and Ethiopia, the retrogressive erosion rate in this region is smaller, but the erosion volume is far greater than in the above-mentioned regions. Affected by precipitation, the gully erosion volume in Southwest Iran is smaller; affected by local slope, land-use type and soil erodibility, the retrogressive erosion of the gully heads in the three agroecosystems in Ethiopia has a great contribution in sediment yields from gullies [19,49], different from the research findings of Guan et al. [50] in the loess hilly and gully region that the forward erosion volume of gully heads took up a proportion far greater than did the spreading volume of gully cliffs due to the effect of the basin area on the dissected valleys studied by them. This study suggests that the increase in gully width leads to increases in both area and volume and that the crosswise widening of gullies has a great contribution in sediment yields from gullies. The gullies within this study area were teeming mainly with croplands on both sides, with low vegetation coverage. Also, the “soil-rock dual structure” of the soil texture has significantly affected the development and evolution of gullies.

Table 5. Development rates of gully erosion in different erosion areas.

Study Area	Major Soil Type	Times	Growth Rates	Author (Year)
Loess Plateau	Loess	62	0.54 m/a (L) 58.3 m ³ /a (V)	Guan et al. [50]
Loess Hilly and Gully Region	Loess	14	0.27 m/a (L) 0.004 m/a (W)	Yang et al. [51]
Southwest of Iran	Fars Lithological Groups	15	1.23 m/a (L) 6.70 m ³ /a (V)	Samani et al. [49]
Tunisia	Calcil or Chromic Vertisols	50	68 m ³ /a (V)	Slimane et al. [16]
Upper Blue Nile basin, Ethiopia	Acrisols and Leptosols (Guder)	11	0.76 m/a (L) 6.77 m ³ /a (V)	Yibeltal et al. [19]
	Leptosols and Luvisols (Aba Gerima)		2.09 m/a (L) 19.58 m ³ /a (V)	
	Vertisols and Luvisols (Dibatie)		3.42 m/a (L) 42.16 m ³ /a (V)	
This Study Area	Soil-Rock Dual Structure	7	0.23 m/a (L) 0.25 m/a (TW) 0.09 m/a (D) 81.58 m ³ /a (V)	



Figure 11. An example of lateral erosion and downcutting erosion in a gully.

The gully erosion in the Yimeng mountain area is subject to the joint influence of multiple factors including vegetation, slope, slope length, soil property, land use type and human activities. The research results will lay a theoretical groundwork for erosion gully treatment, water soil conservation and ecological restoration in the Yimeng mountain area and even in regions with a “soil-rock dual structure”. However, this study only focused on the gully erosion evolution in this region during 2014–2021, rather than on the roles of its influencing factors. Different time scales may lead to slight differences in gully development rate in the Yimeng mountain area. In the future, gully development and evolution patterns could be explored by expanding the time scale and selecting several different time stages.

5. Conclusions

In this study, the erosion rates and erosion amounts of gullies in the Yimeng mountain area, a typical area of “soil-rock dual structure”, were estimated based on the data of a 3D model and high-resolution RS stereopair images. Unmanned aerial vehicle RS imagery was used to correct the errors in gully length (L), top width (TW), depth (D) and area (A) acquired by high-resolution RS imagery, so that the relative errors all fell below 0.005% after correction. After correction, the accuracy of single gully L , TW , D and A in 2014 and 2021 were improved by 1.20–2.64 m, 0.09–1.11 m, 1.19–1.67 m and 0.74–812 m², respectively. Within the 7a from 2014 to 2021, the parameters L , TW and D of all 43 gullies changed to varying degrees, corresponding to an average development rate of 0.23 m/a, 0.25 m/a and 0.09 m/a, respectively. Among them, TW changed most significantly, and the lateral erosion development experienced by the gullies far outweighed the downcutting erosion. The optimal volume model $V = 0.0513 A^{1.4535}$, with $R^2 = 0.944$, was built and screened out according to the UAV RS images, and the gully volumes were calculated in combination with the gully area correction model. Amid the 7a, 90.7% of the 43 gullies within the study area experienced an increase in volume. Considering the gullies alone that experienced the increase in volume, each gully had a volume increment of 571.05 m³ on average. The gully erosion rate within the study area ranges between 0.42 m³/a and 399.39 m³/a, and the total erosion volume of all gullies is 3181.56 m³/a. In the future, the study area could be enlarged and diversified to accommodate further exploration of the influences of vegetation coverage, “soil-rock dual structure”, and other factors on the development and evolution of gullies, so as to provide methods and theoretical support for studying the dynamic change of gullies in large-dimensional “soil-rock dual structure” water-eroded regions using RS data.

Author Contributions: Conceptualization, W.Z.; methodology, W.Z. and G.Z.; software, G.Z.; validation, G.Z.; formal analysis, G.Z. and T.Y.; investigation, W.Z., G.Z., T.Y., W.Q. and X.M.; resources, W.Z.; data curation, W.Z., G.Z., T.Y., W.Q. and X.M.; writing—original draft preparation, G.Z.; writing—review and editing, W.Z. and G.Z.; visualization, T.Y.; supervision, W.Z.; project administration, W.Z.; funding acquisition, W.Z. All authors have read and agreed to the published version of the manuscript.

Funding: This study was supported by the National Natural Science Foundation of China (41907050, 41877073); the Natural Science Foundation of Shandong Province (ZR2019MD031); and the Shandong Colleges and Universities Scientific Research Program (J18KA197).

Data Availability Statement: The data presented in this study are available on request from the corresponding author.

Acknowledgments: The authors thank Fujin Xu, Zhikang Gao, Sizheng Wu, and Zhenghui Lv for their assistance with fieldwork.

Conflicts of Interest: The authors declare no conflict of interest.

References

1. Azareh, A.; Rahmati, O.; Rafiei-Sardooi, E.; Sankey, J.B.; Lee, L.; Shahabi, H.; Ahmad, B.B. Modelling gully-erosion susceptibility in a semi-arid region, Iran: Investigation of applicability of certainty factor and maximum entropy models. *Sci. Total Environ.* **2019**, *655*, 684–696. [[CrossRef](#)] [[PubMed](#)]
2. Omid, R.; Zahra, K.; Sofia, F.C.; Chen, W.; Masoud, S.S.; Marijana, K.S.; Samaneh, S.; Navid, G.; Nader, K. Contribution of physical and anthropogenic factors to gully erosion initiatio. *Catena* **2022**, *210*, 105925.
3. Poesen, J.; Nachtergaele, J.; Verstraeten, G.; Valentin, C. Gully erosion and environmental change: Importance and research needs. *Catena* **2003**, *50*, 91–133. [[CrossRef](#)]
4. Anderson, R.L.; Rowntree, K.M.; Roux, J.J.L. An interrogation of research on the influence of rainfall on gully erosion. *Catena* **2021**, *206*, 105482. [[CrossRef](#)]
5. Arabameri, A.; Pradhan, B.; Bui, D.T. Spatial modelling of gully erosion in the Ardib River Watershed using three statistical-based techniques. *Catena* **2020**, *190*, 104545. [[CrossRef](#)]
6. Bartley, R.; Poesen, J.; Wilkinson, S.; Vanmaercke, M. A review of the magnitude and response times for sediment yield reductions following the rehabilitation of gullied landscapes. *Earth Surf. Process. Landf.* **2020**, *45*, 3250–3279. [[CrossRef](#)]
7. Chowdhuri, I.; Pal, S.C.; Arabameri, A.; Saha, A.; Chakraborty, R.; Blaschke, T.; Pradhan, B.; Band, S.S. Implementation of artificial intelligence-based ensemble models for gully erosion susceptibility assessment. *Remote Sens.* **2020**, *12*, 3620. [[CrossRef](#)]
8. Lucà, F.; Conforti, M.; Robustelli, G. Comparison of GIS-based gullying susceptibility mapping using bivariate and multivariate statistics: Northern Calabria, South Italy. *Geomorphology* **2011**, *134*, 297–308. [[CrossRef](#)]
9. Millares, A.; Díez-Minguito, M.; Moñino, A. Evaluating gullying effects on modeling erosive responses at basin scale. *Environ. Model. Softw.* **2019**, *111*, 61–71. [[CrossRef](#)]
10. Rahmati, O.; Tahmasebipour, N.; Haghizadeh, A.; Pourghasemi, H.R.; Feizizadeh, B. Evaluating the influence of geo-environmental factors on gully erosion in a semi-arid region of Iran: An integrated framework. *Sci. Total Environ.* **2017**, *579*, 913–927. [[CrossRef](#)]
11. Peng, X.D.; Dai, Q.H.; Yang, Z.; Zhao, L.S. Sediment yield of surface and underground erosion in the process of rocky desertification of Karst Area. *Acta Pedol. Sin.* **2016**, *53*, 1237–1248.
12. Belayneh, M.; Yirgu, T.; Tsegaye, D. Current extent, temporal trends, and rates of gully erosion in the Gumara watershed, Northwestern Ethiopia. *Glob. Ecol. Conserv.* **2020**, *24*, e01255. [[CrossRef](#)]
13. Brecheisen, Z.S.; Richter, D.D. Gully-erosion estimation and terrain reconstruction using analyses of microtopographic roughness and LiDAR. *Catena* **2021**, *202*, 105264. [[CrossRef](#)]
14. Castillo, C.; Gómez, J.A. A century of gully erosion research: Urgency, complexity and study approaches. *Earth-Science Reviews* **2016**, *160*, 300–319. [[CrossRef](#)]
15. Frankl, A.; Stal, C.; Abraha, A.; Nyssen, J.; Rieke-Zapp, D.; Wulf, A.D.; Poesen, J. Detailed recording of gully morphology in 3D through image-based modelling. *Catena* **2015**, *127*, 92–101. [[CrossRef](#)]
16. Slimane, A.B.; Raclot, D.; Rebai, H.; Bissonnais, Y.L.; Planchon, O.; Bouksila, F. Combining field monitoring and aerial imagery to evaluate the role of gully erosion in a Mediterranean catchment (Tunisia). *Catena* **2018**, *170*, 73–83. [[CrossRef](#)]
17. Wang, J.X.; Zhang, Y.; Deng, J.Y.; Yu, S.W.; Zhao, Y.Y. Long-Term Gully Erosion and Its Response to Human Intervention in the Tableland Region of the Chinese Loess Plateau. *Remote Sens.* **2021**, *13*, 5053. [[CrossRef](#)]
18. Wang, J.X.; Fan, C.H.; Zhang, Y.; Li, Z. Gully head activity and its influencing factors in China's Loess Plateau. *J. Soils Sediments* **2022**, *22*, 1792–1803. [[CrossRef](#)]
19. Yibeltal, M.; Tsunekawa, A.; Haregeweyn, N.; Adgo, E.; Meshesha, D.T.; Masunaga, T.; Tsubo, M.; Billi, P.; Ebabu, K.; Fenta, A.A.; et al. Morphological characteristics and topographic thresholds of gullies in different agro-ecological environments. *Geomorphology* **2019**, *341*, 15–27. [[CrossRef](#)]
20. Yuan, M.T.; Zhang, Y.; Zhano, Y.Y.; Deng, J.Y. Effect of rainfall gradient and vegetation restoration on gully initiation under a large-scale extreme rainfall event on the hilly Loess Plateau: A case study from the Wuding River basin, China. *Sci. Total Environ.* **2020**, *739*, 140066. [[CrossRef](#)]
21. Castillo, C.; Pérez, R.; James, M.R.; Quinton, J.N.; Taguas, E.V.; Gómez, J.A. Comparing the Accuracy of Several Field Methods for Measuring Gully Erosion. *Soil Sci. Soc. Am. J.* **2012**, *76*, 1319–1332. [[CrossRef](#)]
22. Cook, K.L. An evaluation of the effectiveness of low-cost UAVs and structure from motion for geomorphic change detection. *Geomorphology* **2017**, *278*, 195–208. [[CrossRef](#)]
23. Krenz, J.; Greenwood, P.; Kuhn, N.J. Soil Degradation Mapping in Drylands Using Unmanned Aerial Vehicle (UAV) Data. *Soil Syst.* **2019**, *3*, 33. [[CrossRef](#)]
24. Hosseinalizadeh, M.; Kariminejad, N.; Rahmati, O.; Keesstra, S.; Alinejad, M.; Behbahani, A.M. How can statistical and artificial intelligence approaches predict piping erosion susceptibility? *Sci. Total Environ.* **2019**, *646*, 1554–1566. [[CrossRef](#)] [[PubMed](#)]
25. Kariminejad, N.; Rossi, M.; Hosseinalizadeh, M.; Pourghasemi, H.R.; Santosh, M. Gully head modelling in Iranian Loess Plateau under different scenarios. *Catena* **2020**, *194*, 104769. [[CrossRef](#)]
26. Napoleon, G.E.; Trent, B.; Carlos, C.; Ronald, B.; Eddy, L.; Kristine, T.; Thomas, K.; Yuan, Y.P.; Douglas, L. Measuring ephemeral gully erosion rates and topographical thresholds in an urban watershed using unmanned aerial systems and structure from motion photogrammetric techniques. *Land Degrad. Dev.* **2018**, *29*, 1896–1905.

27. Zhang, Y.; Zhao, Y.Y.; Liu, B.Y.; Wang, Z.Q.; Zhang, S. Rill and gully erosion on unpaved roads under heavy rainfall in agricultural watersheds on China's Loess Plateau. *Agric. Ecosyst. Environ.* **2019**, *284*, 106580. [[CrossRef](#)]
28. Li, Z.; Zhang, Y.; Zhu, Q.K.; Yang, S.; Li, H.J.; Ma, H. A gully erosion assessment model for the Chinese Loess Plateau based on changes in gully length and area. *Catena* **2017**, *148*, 195–203. [[CrossRef](#)]
29. Capra, A.; Mazzara, L.M.; Scicolone, B. Application of the EGEM model to predict ephemeral gully erosion in Sicily, Italy. *Catena* **2004**, *59*, 133–146. [[CrossRef](#)]
30. Caraballo-Arias, N.A.; Conoscenti, C.; Stefano, C.D.; Ferro, V.; Gómez-Gutiérrez, A. Morphometric and hydraulic geometry assessment of a gully in SW Spain. *Geomorphology* **2016**, *274*, 143–151. [[CrossRef](#)]
31. Li, Z.; Zhang, Y.; Shang, G.F.; Qi, F.; Ma, Q.T.; Li, Y.K. Characterizing gully cross section and modelling gully volume in hilly loess region of Western Shanxi Province. *Trans. Chin. Soc. Agric. Eng.* **2018**, *34*, 152–159.
32. Li, Z.; Qi, Z.G.; Qin, W.; Chen, C.; Wu, K.; Feng, T. Gully volume estimation model using high-resolution satellite imaging in mountainous and hilly regions with black soil of Northeast China. *Trans. Chin. Soc. Agric. Eng.* **2021**, *37*, 122–130.
33. Olutoyin, F.; Rotimi, O.; Adeyemi, O.; Deirdre, D. Factors controlling gully morphology on the quartzite ridges of Ibadan, Nigeria. *Catena* **2022**, *212*, 106127.
34. Dong, Y.F.; Xiong, D.H.; Su, Z.A.; Li, J.J.; Yang, D.; Zhai, J.; Lu, X.N.; Liu, G.C.; Shi, L.T. Critical topographic threshold of gully erosion in Yuanmou dry-hot valley in Southwestern China. *Phys. Geogr.* **2013**, *34*, 50–59. [[CrossRef](#)]
35. Zhang, Y.; Gao, C.Y.; Yang, J.; Zhang, Q.; Wang, J.X. Estimating the gully growth rate in the hilly Loess Plateau using historical satellite images. *Trans. Chin. Soc. Agric. Eng.* **2022**, *38*, 109–116.
36. Frankl, A.; Poesen, J.; Scholiers, N.; Jacob, M.; Haile, M.; Deckers, J.; Nyssen, J. Factors controlling the morphology and volume (V)–length (L) relations of permanent gullies in the Northern Ethiopian Highlands. *Earth Surface Processes and Landforms* **2013**, *38*, 1672–1684. [[CrossRef](#)]
37. Kompani-Zare, M.; Soufi, M.; Hamzehzarghani, H.; Dehghani, M. The effect of some watershed, soil characteristics and morphometric factors on the relationship between the gully volume and length in Fars Province, Iran. *Catena* **2011**, *86*, 150–159. [[CrossRef](#)]
38. Xu, F.J.; Zhao, W.J.; Yan, T.T.; Qin, W.; Chen, H.N. Can slope spectrum information entropy replace slope length and steepness factor: A case study of the rocky mountain area in northern China. *Catena* **2022**, *212*, 106047. [[CrossRef](#)]
39. An, J.; Liu, Q.J. Soil aggregate breakdown in response to wetting rate during the inter-rill and rill stages of erosion in a contour ridge system. *Catena* **2017**, *157*, 241–249. [[CrossRef](#)]
40. Liu, B.Y.; Yang, Y.; Lu, S.J. Discriminations on common soil erosion terms and their implications for soil and water conservation. *Sci. Soil Water Conserv.* **2018**, *16*, 9–16.
41. Casali, J.; Giménez, R.; Campo-Bescós, M.A. Gully geometry: What are we measuring? *Soil* **2015**, *1*, 509–513. [[CrossRef](#)]
42. Liu, C.X. Relationship between the volume of gully and the first and second dimension parameters in Yuanmou dry-hot valley. Master's Thesis, China West Normal University, Nanchong, China, 2017.
43. Li, Z.; Zhang, Y.; Yang, S.; Zhu, Q.K.; Wu, J.H.; Ma, H.; He, Y.M. Error assessment of extracting morphological parameters of bank gullies by manual visual interpretation based on QuickBird imagery. *Trans. Chin. Soc. Agric. Eng.* **2014**, *30*, 179–186.
44. Tang, J.; Zhang, Y.; Fan, C.H.; Cheng, X.X.; Deng, J.Y. Accuracy assessment of gully morphological parameters from high resolution remote sensing stereoscopic satellite images on hilly Loess Plateau. *Trans. Chin. Soc. Agric. Eng.* **2017**, *33*, 111–117.
45. He, F.H.; Gao, B.J.; Wang, H.Z.; Wang, R.; Sai, L.L. Study on the relationship between gully erosion and topographic factors based on GIS in small watershed of Jiaodong Peninsula. *Geogr. Res.* **2013**, *32*, 1856–1864.
46. Nash, J.E.; Sutcliffe, J.V. River flow forecasting through conceptual models. *J. Hydrol.* **1970**, *10*, 282–290. [[CrossRef](#)]
47. Deng, Q.C.; Qin, F.C.; Zhang, B.; Wang, H.P.; Luo, M.L.; Shu, C.Q.; Liu, H.; Liu, G.C. Characterizing the morphology of gully cross-sections based on PCA: A case of Yuanmou dry-hot valley. *Geomorphology* **2015**, *228*, 703–713. [[CrossRef](#)]
48. Geng, Y.H. *Treatment of Typical Sloping Farmland Erosion Ditch in Black Soil Region*; Hei Long Jiang University: Harbin, China, 2021.
49. Samani, A.N.; Rad, F.T.; Azarakhshi, M.; Rahdari, M.R.; Rodrigo-Comino, J. Assessment of the Sustainability of the Territories Affected by Gully Head Advancements through Aerial Photography and Modeling Estimations: A Case Study on Samal Watershed, Iran. *Sustainability* **2018**, *10*, 2909. [[CrossRef](#)]
50. Guan, Y.B.; Yang, S.T.; Zhao, C.S.; Lou, H.Z.; Chen, K.; Zhang, C.B.; Wu, B.W. Monitoring long-term gully erosion and topographic thresholds in the marginal zone of the Chinese Loess Plateau. *Soil Tillage Res.* **2021**, *205*, 104800. [[CrossRef](#)]
51. Yang, L.H.; Pang, G.W.; Yang, Q.K.; Pei, Z.L.; Wang, L.; Long, Y.Q.; Wang, C.M. Changes and influencing factors of erosion gully in Wangmaogou watershed in the last 50 years. *J. Soil Water Conserv.* **2020**, *34*, 64–70.

Disclaimer/Publisher's Note: The statements, opinions and data contained in all publications are solely those of the individual author(s) and contributor(s) and not of MDPI and/or the editor(s). MDPI and/or the editor(s) disclaim responsibility for any injury to people or property resulting from any ideas, methods, instructions or products referred to in the content.